Journal Pre-proof

Faulting, sediment loading, and flow of underlying ductile units: A case study from the Western Ionian Basin Offshore Eastern Sicily

S. Gambino, G. Barreca, F. Gross, G.I. Alsop, C. Monaco

PII: S0191-8141(23)00149-9

DOI: https://doi.org/10.1016/j.jsg.2023.104932

Reference: SG 104932

To appear in: *Journal of Structural Geology*

Received Date: 26 May 2023

Revised Date: 28 July 2023

Accepted Date: 5 August 2023

Please cite this article as: Gambino, S., Barreca, G., Gross, F., Alsop, G.I., Monaco, C., Faulting, sediment loading, and flow of underlying ductile units: A case study from the Western Ionian Basin Offshore Eastern Sicily, *Journal of Structural Geology* (2023), doi: https://doi.org/10.1016/j.jsg.2023.104932.

Author contributions

Gambino Salvatore: conceptualization, Methodology, Formal analysis, Investigation, Writing - Original Draft, Visualization. Barreca Giovanni: conceptualization, Formal analysis, Investigation, Writing - Review & Editing, Visualization, Funding acquisition. Gross Felix: Writing - Review & Editing, Data Curation. Alsop Ian: Writing - Review & Editing. Monaco Carmelo: Resources, Writing - Review & Editing.

Faulting, sediment loading, and flow of underlying ductile units: a case study from the Western Ionian Basin Offshore Eastern Sicily

Gambino S.[1,2], Barreca G.[1,2], Gross F.[3,4], Alsop. G.I.[5] and Monaco C.[1,2,6]

1. Department of Biological, Geological and Environment Sciences, University of Catania, Catania, Italy
2. CRUST—Interuniversity Centre for 3D Seismotectonics with Territorial Applications, Chieti, Italy
3. Institute of Geosciences, Kiel University, Kiel, Germany
4. Center for Ocean and Society, Kiel University, Kiel, Germany
5. Department of Geology & Geophysics, University of Aberdeen, Scotland, UK
6. Istituto Nazionale di Geofisica e Vulcanologia, Etneo, Catania, Italy

Corresponding author: Gambino Salvatore (salvatore.gambino@unict.it)

Keywords: Syn-depositional deformation, ductile flow, turbidite basin, Western Ionian Basin

Abstract

Tectono-stratigraphic analysis coupled with digital 3D surface modelling derived from high-resolution seismic profiles is performed along a narrow turbidite basin offshore E-Sicily to increase understanding on the processes that contributed to the shaping of the Western Ionian Basin. Seismic-reflector patterns of the identified Pliocene-Quaternary sequence point to syn-depositional deformation during the Pliocene associated with the simultaneous activity of regional faults and underlying ductile units. Long-wavelength sediment fanning results from the extensional activity of the Malta Escarpment faults. Conversely, internal reflector architecture and lateral terminations indicate localized subsidence associated with the growth of uprising structures in the easternmost part of the basin. Lateral shifting of basin depocenters is in line with withdrawal effects observed in basins floored by ductile units (salt or shale). 3D modelling of time-reference surfaces highlights sub-circular depressions associated with nearby structural culminations. This pattern is similar to salt-withdrawal minibasins commonly reported in evaporite-floored basins. Accordingly, salt migration/flow triggered by sediment loading, locally enhanced by fault activity, is proposed as the process controlling basin evolution during the Pliocene in the Western Ionian Domain. Nevertheless, the possibility of shale/mud tectonics as ductile source of deformation cannot be discounted.

1. Introduction

Patterns of sedimentation within basins formed along continental margins are generally governed by a number of factors among which regional tectonic instability and climate changes may play a significant role. Apart from these large-scale processes, other local factors such as basin-bounding-fault activity, subsidence by sediment loading, and the occurrence of mobile material in the sedimentary record may also control the internal architecture of a basin (Gemmer et al., 2004; Wood, 2010; Ge et al., 2020; Rojo et al., 2020). In basin analysis, discriminating between these factors is however challenging and additional methods and approaches are required to address the issue. When combined in a suitable workflow, subsurface imaging along with 3D modellingmay help in this regard providing powerful tools to (i) successfully interpret the tectono-stratigraphic evolution of a basin and (ii) discriminate between processes that have contributed to the final basin architecture.

The Calabrian Accretionary Wedge (hereinafter CAW), in the eastern Mediterranean Basin (Fig. 1a and b), formed during the Nubia-Eurasia plate convergence in response to the subduction of the Ionian oceanic lithosphere beneath the European margin (Minelli & Faccenna, 2010; Polonia et al., 2011). The wedge is currently sandwiched between the Calabrian backstop (upper plate) to the North and the still underplating Ionian crust (lower plate) to the South (see schematic cross-section in Fig. 1e). Within this framework, the CAW has been internally deformed and pushed toward the African foreland. The migration of the CAW outer front is favoured by the occurrence of Messinian evaporites that act as a basal detachment (see Minelli & Faccenna, 2010; Valenti, 2010; Polonia et al., 2011).

The CAW presently forms a large (250 x 250 km-wide) fold and thrust system in the Ionian Sea where sediments, scraped from the top of the descending Ionian oceanic crust, have been tectonically stacked (in the last 6-5 Myr, see Gutscher et al., 2016), giving rise to a complicated tectono-stratigraphic setting of the accretionary wedge. According to available literature (Minelli & Faccenna, 2010; Polonia et al., 2011; Gallais et al., 2012), the wedge is divided into an inner and outer part: the Pre-Messinian wedge and the Post-Messinian wedge respectively (Fig. 1a). The Pre-

Messinian wedge includes stacks of Mesozoic-Tertiary units migrating over a basal detachment at the top of the Mesozoic carbonates. Conversely, the more advanced post-Messinian wedge is formed of Plio-Quaternary units confined at depth by a basal detachment located within the Messinian evaporites (see Valenti, 2010 and schematic cross-section in Fig. 1e).

The CAW front, currently about 250 km SE from the Calabrian backstop, exhibits a lobe-shaped geometry and it is surrounded by foredeep basins such as the Ionian Abyssal Plain in the South (Tugend et al., 2019; see Fig. 1a). Here, youngest basin-fill sequences, drilled at DSDP Site 374 (Hsu et al., 1978), consist of Messinian evaporites and Pliocene-Quaternary terrigenous and turbidite sediments. A still unshortened branch of the foreland basin also occurs to the West of the CAW front in the near-offshore of Eastern Sicily (see Fig. 1b and schematic cross-section in Fig. 1d). This roughly N-S elongated marine basin, named the 'Turbidite Valley' (Gutscher et al., 2016; Rebesco et al., 2021, Fig. 1b), is filled by Pliocene-Quaternary turbidite sediments with evidence of E-W extension rather than compression (as might be expected close to the front of the wedge). Sequential restoration analysis previously performed over the turbidite basin (Gambino et al., 2022a) indicates an uneven deformation rate during the Pliocene. A diffuse extensional strain, in the order of 0,2-0,4 mm/yr, affected the basin during the Messinian-lower Pliocene transition and decreased over-time before strain localized on major faults (Gambino et al., 2022a). This anomalously high extensional rate in the early stage of basin shaping was thought by these authors to be caused by plastic deformation occurring in the basin-flooring Messinian units, although this topic was not addressed in detail.

Internal adjustment of basins due to migration of ductile units (e.g., salt or shale) driven by sediment loading have been widely observed around the globe (Ge et al., 2020) and in the Mediterranean domain as well (Loncke et al., 2006; Reiche et al., 2014; Soto et al., 2022). The occurrence in the sedimentary sequence of salt and shales/mud (Barreca, 2014; Butler et al., 2014; Polonia et al., 2017; Dellong et al., 2020), buried under a significant thickness of sediments (as in the case of the CAW surrounding basins), may play a significant role on the patterns of sedimentation and deformation within the basin.

Our goal in this study is to understand if non-tectonic processes have operated in the shaping of the Western Ionian Basin, and if so, how they have affected detailed stratigraphic geometries. We address this issue via a targeted analysis of seismic reflector patterns performed over parts of a set of previously interpreted high-resolution seismic lines (see Gambino et al., 2021, 2022 a,b), which were also exploited as baseline findings to support the novel outcomes from the present paper. We also present additional basin analysis generated by 3D modelling of time-reference surfaces which enables a better insight into the spatial-temporal deformation experienced by the basin. This combined approach allows us to now depict the Pliocene evolution of the turbidite basin in relation to flow of viscous material under increasing sediment loading. This study also opens stimulating research perspectives that may enable future investigations in the Mediterranean area focussing on large salt-shale floored basins where the impact of flowing ductile material on sediment patterns and fault nucleation/activity is still poorly explored.

(Please insert Fig.1 here)

2. Geological setting

2.1. General outlines

The Ionian Basin is a remnant of a Mesozoic oceanic domain connected to the Permo-Triassic opening of the Neo-Tethys Ocean (Şengör, 1979), and it is considered the oldest sea rooted by an "in situ" oceanic crust (Speranza et al., 2012; Dannowski et al., 2019). The Ionian oceanic lithosphere began to subduct beneath the European margin 35 Ma ago (Malinverno & Ryan, 1986; Jolivet & Faccenna, 2000). After that, subduction was characterized by slab roll-back, trench migration toward the SE, and opening of large back-arc basins (see Faccenna et al., 2014 and references therein). All of these geodynamic processes finally contributed to the intricate tectonic evolution of the

Mediterranean region. Lateral tearing (Govers & Wortel, 2005; Barreca et al., 2016; Gutscher et al., 2016) also accompanied roll-back dynamics leading to the progressive narrowing of the subducting Ionian slab (Schellart et al., 2007; Rosenbaum et al., 2008). The active portion of the subduction system is currently confined between southern Calabria and north-eastern Sicily (Scarfì et al., 2018). Migration toward the African foreland of the Calabrian backstop, along with subduction of the Ionian lithosphere, have led to the shaping of a large accretionary prism in the Ionian Sea, the Calabrian Accretionary Wedge (CAW, see Fig. 1).

The CAW, emplaced between the Apulian margin to the NE and the Malta Escarpment in the SW, consists of a stack of SE-verging thrust sheets made up of Mesozoic-Cenozoic sediments originally deposited over the Ionian oceanic domain (Finetti, 1982; Cernobori et al., 1996; Catalano et al., 2001). Pliocene-Quaternary sedimentary units are deformed and piled-up along the more advanced portion of CAW where they form a relatively shallow fold and thrust system (Polonia et al., 2011). Tectonic shortening is here mostly accommodated along a basal detachment favoured by the occurrence of thick evaporitic layers. To the West, the CAW is bounded by the Malta Escarpment (hereafter MESC), a 300 km-long structural discontinuity inherited from the Permo-Triassic paleogeography (Scandone, 1981) along which the Mesozoic Hyblean sequences were stretched and strongly down-faulted. The MESC hanging-wall basin was later filled by Cenozoic sediments (Micallef et al., 2018; Dellong et al., 2020; Rebesco et al., 2021) and currently it forms a narrow (7-10 km wide) and long (>50 km) corridor confined between the front of the CAW and the MESC slope (Gutscher et al., 2016; Micallef et al., 2018; Gambino et al., 2021; Rebesco et al., 2021). The turbidite basin can be considered part of a foreland basin controlled by the activation of normal faults in the lower plate of the collisional system. Seismic imaging across the basin (Gutscher et al., 2016; Micallef et al., 2018; Rebesco et al., 2021), along with sediment waves found at various depths, (see Fig. 3b), reveals it as a Pliocene-Quaternary turbidite system mostly fed from the North. Another sediment source is represented by the steep MESC slope (Fig. 1c) as testified by Pliocene-Quaternary sediments dredged and cored along it (Scandone, 1981).

The turbidite basin is internally deformed by extensional tectonics (Gutscher et al., 2016; Gambino et al., 2021, 2022b), and has escaped compression related to the CAW front. The advancement in the area (toward the West) of the CAW front was probably inhibited by inherited NE-dipping, Meso-Cenozoic extensional structures bordering the Alfeo Seamount block to the NE (see Maesano et al., 2020). These inherited structures were reused during Quaternary times by the propagation of a large NW-SE trending wrench fault system (North Alfeo Fault, NAF, see Gutscher et al., 2016 also known as the Alfeo-Etna Fault, Polonia et al., 2016; Gambino et al., 2022b - Fig. 1) that currently represents a boundary between the contractional domain of the wedge (to the East) from the extensional one (to the West). According to available literature (Butler et al., 2014; Micallef et al., 2018; Camerlenghi et al., 2020), a ~1 sec. T.W.T.-thick evaporite layer flooring the investigated basin is inferred from geophysical data. Wide-angle seismic data across the Western Ionian Basin (Dellong et al., 2018), also reveals the occurrence of a high seismic velocity body (`4.3 km/s) at a depth of 3-6 km that is interpreted as 1-2 km-thick evaporite layer.

2.2. The MESC fault activity

The MESC faults, bounding the turbidite basin to the west (Fig. 1b), have been the focus of investigations in the past decades due to their seismotectonic nature and associated hazards (Scicchitano et al., 2022 and references therein). At the base of the MESC slope, a 250 m-high scarp has been produced by the activity of three main fault splays (F1, F2 and F3 referred as MESC faults, see Gambino et al., 2021). The recent activity of MESC faults has been highlighted by offshore geophysical data that shows steep fault scarps and Pliocene-Pleistocene sediment thickening (Scandone, 1981 and references therein). Further investigations in the early 2000s (Bianca et al., 1999; Argnani & Bonazzi, 2005), provided insights on the seismotectonics and fault tectonic rates deforming the Western Ionian basin. According to last authors, the Quaternary reactivation of the MESC involved only the northern portion of the MESC discontinuity with an estimated vertical rate up to 3.7 mm/yr. The kinematics of the MESC faults has been a matter of debate for the last 30 years following the December 13, 1990, M_L=5.4 earthquake. Available focal mechanisms (Amato et al., 1995) suggest left-lateral kinematics on a rougly N-S trending nodal plane. This trend generally contrasts with the geodetic (D'Agostino & Selvaggi, 2004; Mattia et al., 2012; Palano et al., 2012), structural (Monaco & Tortorici, 2000; Cultrera et al., 2015), and borehole breackout data (Ragg et al., 1999; Montone et al., 2012), that suggest a right-lateral transtensional kinematics for the MESC faults.

High-resolution seismic profiles and bathymetric data (Gutscher et al., 2016, 2017) provide a better sub-seafloor imaging and seabed expression of the ~ 60 km long MESC fault system. Exploiting these data, Gambino et al., (2021, 2022a) redefined faults vertical tectonic rates (i.e., 0.1-0.4 mm/yr for the Pliocene, and 3 - 7 mm/yr for the Quaternary). The double-bell-shaped throw/distance patterns computed for the three fault splays (F1, F2, and F3) , suggests that,during the Messinian-lower Pliocene (see Fig.4a), each fault splay nucleated as two separated segments and after, during the Quaternary, they merged into a single tectonic structure.

3. Data and Methods

High-resolution seismic lines from different marine expeditions (Poseidon cruise POS496, R/V Poseidon, March–April 2016, see Krastel, 2016, and the CIRCEE-HR cruise, R/V le Suroît, October 2013, see Gutscher et al., 2016), have been used in our work to explore the sub-seafloor tectono-stratigraphic setting of the turbidite basin. Seismic data acquisition and processing workflows are reported in the quoted literature for detailed information. The two seismic datasets were integrated with other published seismic lines (Argnani & Bonazzi, 2005; Argnani et al., 2012; Gutscher et al., 2016; Polonia et al., 2016, 2017) to spatially cover the entire turbidite basin and to perform 3D modelling. Tectono-stratigraphic interpretation over the seismic datasets was initially based on seismic facies analysis (amplitude, lateral continuity, and frequency of internal reflectors) and then on picking the main discontinuities bounding seismic units with homogenous seismic characters (see section 4.1). A TWT/Depth conversion was then applied to all the interpreted seismic datasets using a velocity model achieved from available literature (Kokinou et al., 2003; Gallais et al., 2011; Butler et al., 2014; Maesano et al., 2017; Micallef et al., 2018; Camerlenghi et al., 2020) and summarised in Tab.1. The 2D linear discontinuities were spatially interpolated through common statistical methods (Kriging) to obtain pseudo-3D surfaces of selected horizons (S2 and S3, see section 5). Seismic data interpretation, TWT/Depth conversion, and 3D modelling were performed using the MOVE 2020.1 software package (Petex Ltd.).

4. Basin analysis of the Pliocene-Quaternary section

A detailed basin analysis was performed over the high-resolution seismic datasets with the aim to better understand the tectono-stratigraphic evolution of the turbidite basin. The analysis was particularly focused on the internal sedimentary pattern to achieve information on what controlled the final shaping of the basin.

4.1. Seismo-stratigraphy

Interpretation of seismic profiles follows previous studies in the area concerning fault activity (Gambino et al., 2021), and sequential restoration methods aimed at assessing the rate of crustal extension in the area (Gambino et al., 2022a). According to the seismic facies analysis performed by Gambino et al., (2021), four main seismo-stratigraphic units were recognized to have filled the turbidite basin during the Pliocene-Quaternary. These seismic units, from the bottom to the top, are Pre-MES, MES, PQ1 and PQ2 (Fig. 2a). The units are bounded by well-defined discontinuities generally consisting of angular unconformities and/or erosive truncations (S1 to S4 in Fig. 2).

(Please insert Fig.2 here)

Pre-MES shows chaotic and locally transparent seismic facies with isolated highly reflective bodies (Fig. 2a). The unit represents a paleo-slope (Malta Escarpment) on which the younger sedimentary units lay with on-lap and/or off-lap terminations (Fig. 2a). The Pre-MES unit is truncated upwards by the S1 discontinuity. Although the MES unit is a rather heterogeneous seismic marker, some low- to medium-amplitude, medium frequency, sub-parallel- to chaotic and discontinuous reflectors are observed (Fig. 2a). Where the units get shallower (i.e., eastwards of NAF), a threefold internal subdivision of the MES unit can be observed (see Fig. 6b). The upper portion is a transparent- to chaotic seismic facies with a high-reflective top-surface. The central portion shows high-reflective and sub-parallel continuous reflectors, while the lower portion again exhibits a transparent- to chaotic seismic marker. The upper limit of the MES unit is an erosive and locally highly-reflective discontinuity (S2) on which the upper units lay in para-conformity and/or onlap geometry (Fig. 2). The PQ1 unit is characterized by low to high-amplitude, low-medium frequency, subparallel and continuous reflectors. Within the turbidite basin, the unit PQ1 shows sediment waves at various depths that indicate a turbiditic infilling of the basin with sediments coming mostly from the North (Fig. 3, see also Rebesco et al., 2021). The PQ1 unit has been further subdivided in three sub-units by Gambino et al., (2022a) (PQ1a, PQ1b and PQ1c) according to S3a and S3b bounding discontinuities (Fig. 2a). The S3 discontinuity is interpreted as an erosive truncation separating PQ1 from the younger PQ2 unit. The PQ2 unit shows high-frequency, high-amplitude, continuous and parallel reflectors that lays unconformably on the PQ1 and locally terminating with onlap geometry.

(Please insert Fig.3 here)

Despite the absence of drill data for the investigated section, seismic facies analysis along with the stratigraphic position of seismic units allows correlation to chrono-stratigraphic sequences drilled in similar marine setting along the Ionian Basin (i.e., in the Ionian abyssal plain, see Hsü et al., 1978) and illuminated by seismic lines (Butler et al., 2014; Micallef et al., 2018; Camerlenghi et al., 2020). Pre-MES seismic facies is coherent with carbonate sequences widely outcropping on land (Hyblean Plateau) and sampled along the MESC slope (Scandone, 1981). The MES unit is interpreted as Messinian deposits for its locally high-reflective top-discontinuity and internal chaotic- to layered markers (Lofi et al., 2011). Moreover, the internal subdivision observed eastward of NAF (Fig. 6b) resembles the threefold subdivision proposed by (Butler et al., 2014). The PQ1 unit correlates with the PQb and PQc units by (Camerlenghi et al., 2020) and partially with the “Unit one” of (Micallef et al., 2018). Moreover, the S3 discontinuity (top-PQ1), correlates with the erosional surface dated by Camerlenghi et al., (2020) at 650 ka (DSDP site 374 cores, (Hsü et al., 1978). In line with previous studies, the PQ1 unit is interpreted as a Pliocene-Quaternary sediment section. The PQ2 unit, laying on the S3 discontinuity, is therefore assumed to be Pleistocene-Holocene in age.

Among the recognized top-reflectors, the S2 and S3 horizons represent reliable time-references since they correlate well with the top of evaporitic units (5.32 Ma, see Hsü et al., 1977; Lofi et al., 2011) and with the ̀650 ka erosive discontinuity (Camerlenghi et al., 2020; Rebesco et al., 2021), respectively. Chrono-stratigraphic interpretation and related seismic velocities (from literature) are reported in Tab. 1.

(Please insert Tab.1 here)

4.2. Depositional architecture

A detailed seismic-stratigraphic analysis was focused on the to the Pliocene-Quaternary sedimentary section and particularly on its pattern of internal reflectors in order to define the depositional evolution of the basin. The basin has been explored transversally through the CIR-01 seismic profile (Fig. 2), and longitudinally through the P701 line (Fig. 3).

The overall geometric pattern of the Pliocene-Quaternary sequence (PQ1 and PQ2 units, Fig.2), in the eastern portion of the basin, is characterized by a slight W-wards fanning of the sediments approaching the F3 fault of the MESC system (Fig. 2a). In the western portion, in the footwall of MESC system, the sediment section appears undisturbed and gently-tilted toward the East according to the MESC slope. Apart from this general pattern that testifies the Pliocene-Quaternary sin-sedimentary activity of MESC faults, sediment down-bending is evident in the easternmost part of the turbidite basin where a trough is observed along the western flank of a folded and uplifted structure limiting the basin to the East (Fig. 2). The reflector's geometry within the PQ1 section indicates localized subsidence that, being far (4-5 km) from the MESC faults (F3), should be associated with another deformation process. Down-bending of sediments is more pronounced in the

S2 horizon (MES top-reflector) and progressively reduces upward as indicated by the geometry of the S3a and S3b horizons.

The PQ1a sub-unit, between S2-S3a (Fig. 2a, b), is characterised by concave-up reflectors with a progressive lateral thinning toward the uplifted area. The more reflective lower part of the PQ1a sub-unit unconformably rests on the MES unit with on-lap geometry (Fig. 2c), whereas the less-reflective upper part appears to drape the uplifted area with a converging geometry of strata. Within the unit, depocenters are observed to migrate eastwards during sedimentation (Fig. 2c). The PQ1b sub-unit, between S3a and S3b discontinuities, is characterised by west-dipping reflectors terminating against the S3a discontinuity with down-lap geometry. Toward the East, the sub-unit is geometrically concordant with the S3a surface and a gentle convergence of reflectors is observed as the unit thins away (Fig. 2c). The PQ1c sub-unit is separated from the previous unit by the highly-reflective S3b discontinuity. The sub-unit appears laterally continuous and its internal reflectors are concordant with the basal S3b horizon. The youngest PQ2 unit is characterized by a sub-horizontal pattern of reflectors and is confined at the base by the erosive S3 discontinuity (Fig. 2a, b).

The P701 seismic profile illuminates the turbidite basin longitudinally for about 45 km from offshore Mt. Etna in the North to Siracusa in the South (Fig. 3). Overall, the P701 seismic profile highlights that S2 and S3 discontinuities are affected by about 15 km-wavelength down-bending, resulting in the shaping of two distinct depocenters ('Troughs' in Fig. 3). Diffused sediment waves and internal unconformities (section 4.1, see also Rebesco et al., 2021) within the PQ1 unit are in line with the turbiditic nature of the basin and their pattern is consistent with a sediment supply from the North. Down-bending is more pronounced in S2 than S3, suggesting that deformation occurred overtime during the deposition of sedimentary sequences. Such a bending is also slightly shown by the Quaternary PQ2 unit, that appears undeformed (horizontal) in Cir-02 (Fig. 2).

Here, we develop a new 3D model of reference horizons (top Messinian and top PQ1 units) with the aim of providing an overview of how deformation may have controlled sediment architecture at basin scale (Fig. 4). Following the seismic-stratigraphic interpretation (see section 4.1 and

Gambino et al., 2021 for the complete interpreted seismic lines dataset), S2 and S3 discontinuities have been used as reference surfaces according to their constrained ages. Interpreted seismic sections have been TWT-to-depth converted following a seismic velocity model based on literature (Tab.1, see Gambino et al., 2022a and references therein). Depth-converted 2D horizons (S2, S3), have been spatially interpolated across the entire seismic database (see section 3 and Fig. 1c for location) using Kriging algorithm. A pseudo-3D model of the selected reference surfaces is thereby obtained (Fig. 4b, c).

(Please insert Fig.4 here)

The S2 modelled surface (top-MES) shows a quite irregular morphology characterized by the occurrence of sub-circular basins and ridges (Fig. 4b). Two lowered areas are resolved in the hanging wall of the F3 fault (MESC system); one located in the central part of the fault, the other about 10 km northward, respectively. Dome-shaped reliefs occur about 15 km SE of the subsided areas and have a comparable areal extension (Fig. 4b).

The S3 surface (Top-PQ1, Fig. 4c), shows slight similarity with the older S2 surface but with a smoother morphology according to deformation reducing upwards (see section 4.2). A thickness map of PQ1 unit is derived by subtracting the depth of S3 from S2 (Fig. 4d). The map highlights how the greatest thickness (>700 m) is resolved along the circle-shaped subsided areas adjacent to the MESC faults (F3). Furthermore, the area with maximum thickness is observed to be located where the maximum throws of MESC faults occur.

5. Data interpretation and Basin evolution

The analysis of depositional patterns reconstructed through the seismic dataset and 3D modelling of reference surfaces, provides constraints for interpreting the Pliocene evolution of the turbidite basin. MESC faults activity influenced part of the basin architecture characterised by long-wavelength sediments fanning toward the West (Fig. 2). However, major effects of deformation in the sediment pattern have been mostly recorded by the PQ1 unit away from the MESC faults. Approaching the uplifted area bounding the basin to the East, syn-kinematic PQ1 deposition is evidenced by the sub-units' internal reflectors pattern and by their lateral terminations that appear primarily controlled by the localized subsidence (Fig. 2, see section 4.2). Onlapping and converging reflectors on the eastern margin of the subsided basin (Fig. 2a), are consistent with a syn-depositional uplift involving the culmination to the east (uplifted area in Fig. 2). Overtime depocenters migration toward the East, observed within the PQ1a sub-unit (Fig. 2c) contrasts with the CAW-front pushing in the opposite-way. Further, the 15 km-long wavelengths folding observed in p701 line (Fig. 3) could not be related to the general N-S compression observed in the accretionary wedge (West of NAF, Fig.1, 2). In fact, the fold-spacing (wavelength) observed within the Calabrian Accretionary Wedge is in the order of 2-5 km, or even less (Valenti, 2010; Polonia et al., 2011; Gutscher et al., 2016), so way shorter than that in the turbidite basin. Accordingly, a different source of deformation should be invoked to explain the depocenters migration pattern and the anomalous down-bending observed along the seismic dataset (e.g., S2 in Fig. 2, 3).

Depocenters migration of PQ1a (Fig. 2c) may suggest the latter deposited over a mobile layer substratum (see also Ge et al., 2020; Rojo et al., 2020). 3D modelling revealed the morphology of reference surfaces, corresponding to the top of Messinian (MES) and Pliocene (PQ1) units, and how Pliocene sediment thickness varies along the turbidite basin. A peculiar point in the reconstructed MES top-surface (S2), is the occurrence of sub-circular troughs systematically associated with dome-shaped culminations in the nearby (toward SE, Fig. 4b). Sub-circular basins and domes morphologies have a comparable dimension, suggesting therefore a cause-effect relation between subsidence and uplift. This pattern resembles salt-withdrawal minibasins commonly observed in evaporite-floored basins (Hudec et al., 2009; Goteti et al., 2012; Ge et al., 2020). In this framework, a syn-kinematic depositional model may be explored in view of the occurrence of mobile layers underlying the analysed turbidite basin, and considering that formation of minibasins generally requires localized sediment loading.

6. Discussion

6.1. General outcomes

A comprehensive basin analysis performed over a turbiditic basin located offshore eastern Sicily revealed that different kinds of deformation have controlled the internal architecture of the infilling Pliocene sediment section. While long-wavelength sediment fanning can be related to the activity of basin extensional faults (MESC system, Fig. 2), localized subsidence in the eastern portion of the basin suggests additional factors may have operated.

Sequential restoration methods previously applied to assess the rate of crustal extension (Gambino et al., 2022a), demonstrates that a high extensional rate was experienced by the basin during its early stage of deformation (Fig. 5a). Moreover, restored sections (Fig. 5b, c) revealed that part of the deformation remained unrestored. In sequential restoration analysis, unresolved (residual) deformation may be associated with out-of-section migration of ductile material or, alternatively, to evaporite dissolution (Rowan & Ratliff, 2012). Following this point, the predicted plastic deformation controlling basin evolution was carefully tested through a detailed sediment pattern analysis and 3D modelling.

(Please insert Fig.5 here)

The internal reflectors' architecture of the whole PQ1 unit (sediment thickening and lateral terminations, Fig. 2c), suggests a coeval subsidence (sinking of S2 and S3 top-surfaces) and uplift in the easternmost portion of the basin (Fig. 2). Moreover, depocenter shifting (black dots in Fig. 2c-right panel) observed within the PQ1a sub-unit indicates a mobilization of the underlying ductile body toward the East. According to previous studies, this process is generally associated with the shaping of withdrawal minibasins widely recognized in salt-bearing basins as observed in the field (Lopez-Mir et al., 2014), seismic profiles (Ge et al., 2020) and predicted by sandbox experiments (Rojo et al., 2020). Ductile migration triggered by sediment load is however reported in the literature both for salt (Brewer & Kenyon, 1996; Goteti et al., 2012; Peel, 2014; Ge et al., 2020; Rojo et al., 2020) and shales tectonics (Soto et al., 2010; Wiener et al., 2010; Wood, 2010). Even though the mechanical behaviour of the involved ductile substrate is different, migration of salt or over-pressured shales may result in similar structures (diapirs, domes, walls, mini-basins etc., see Morley & Guerin, 1996; Wood, 2010).

Information on the nature of the inferred ductile layer under the S2 discontinuity remains elusive since penetration of seismic lines do not aid in this regard. The occurrence of Messinian salt flooring the Western Ionian Basin is however commonly reported in several studies exploiting geophysical data (Butler et al., 2014; Gutscher et al., 2016; Micallef et al., 2018; Camerlenghi et al., 2020). Wide-angle seismic surveys (Dellong et al., 2018), point to a high seismic velocity body (`4.3 km/s) underlying the turbidite basin, interpreted by the authors as an evaporite body. A roughly 1 sec. TWT-thick transparent/chaotic layer is interpreted as a halite layer in the southern part of the Turbidite basin (Butler et al., 2014), and its proposed internal seismic subdivision matches the internal seismic character of the MES unit within the Cir-01 line (Fig. 6b). Nevertheless, over-pressured serpentinite-derived muds have been inferred in the CAW (Polonia et al., 2017) and directly observed on-land along the western margin of the turbidite basin (Manuella et al., 2012; Barreca, 2014).

(Please insert Fig.6 here)

It is worth noting that, shale migration triggered by sediment loading is created when burial is greater than 1 km (Soto et al., 2021), a condition that is not achieved by the turbidite basin during the early Pliocene (at the onset of observed deformation) when the thickness of PQ1a sub-unit was less than 0.5 km (see Tab.1). Progressive sediment accumulation toward the South, also favoured by MESC fault activity, provides the necessary load for withdrawal processes in the underlying MES unit and its consequent lateral migration toward the unconstrained side (i.e., eastern side) of the basin forming, as a whole, basin and dome structures. In particular, effects of lateral inflation such as domes (Fig. 2, 6d) or diapir-like structures (Fig. 6f) occur in the eastern margin of the basin where their emplacement was likely controlled by inherited structural discontinuities, as sand-box experiments suggest (Rojo et al. 2020). Furthermore, the subsequent Quaternary strike-slip deformation (i.e., the NAF system, Gutcher et al., 2016; Polonia et al., 2016; Gambino et al., 2022b, Fig. 6f) exploited these mechanically weak corridors and previous foreland faults to propagate, probably triggering further uprising of ductile material (see Fig. 6d).

Ductile migration of buried salt/shale/mud bodies under sediment loading, and its role in sediment deformation and fault propagation may be of interest in redefining the seismotectonics of salt-floored basin such as the Mediterranean region, especially in areas characterized by high-levels of seismicity, such as the Western Ionian Basin (Gambino et al., 2022b and reference therein). Salt migration and diapirism also imply intense plastic deformation so that preexisting faults in the overlaying sediments could be reactivated. The diagram in Fig. 5a (see also Gambino et al., 2022a) clearly shows that high extensional rates (solid lines in Fig. 5a) related to the ductile migration during the Messinian-Pliocene did not play a significant role on recent MESC fault activity (dashed lines in Fig. 5a). The tectonic origin of MESC faults is consistent with the diverging GPS vectors measured on the lower plate of the collisional system (see Ward 1994; Mastrolembo et al., 2014; D'Agostino and Selvaggi, 2004; Grenerczy et al., 2005), and with raised marine terraces on land on its footwall block (Bianca et al., 1999; Meschis et al., 2021).

6.2. Sediment loading and ductile migration

Localized subsidence, sediment internal pattern and uplift to the East of the investigated turbidite basin, have been interpreted to be produced by migration and relative inflation of salt under sediment loading (Fig. 6). Our interpretation is supported by models of withdrawal minibasins based on natural outcrops (Lopez-Mir et al., 2014), sand-box analogues (Rojo et al., 2020), and numerical simulations (Goteti et al., 2012). The models postulate that sinking of a portion of a basin over a ductile layer may result from sediment loading. Sediment supply and loading may also trigger migration and lateral inflation of underling ductile material (salt, shales, mud) producing a number of structures spanning from plateau, diapirs, (salt-) walls etc. (Wood, 2010; Rojo et al., 2020) among many others. Basin analysis supported by 3D modelling indicates that most of the conditions required for such a mechanism can be found in the investigated basin. Sediment pattern and structural features are also in line with analogue and numerical modelling concerning ductile migration under sediment loading. To support ductile migration in the turbidite basin, the interpreted seismic-stratigraphic pattern has been compared with available analogue simulations dealing with syn-depositional deformation of sediments over a salt layer (Rojo et al. 2020). In particular, our data show strong similarities with syn-kinematic basin deformation shown in Model 1 of Rojo et al. (2020), which simulates salt migration triggered by loading of prograding sediments in a fault-bounded basin (Fig. 5c, e).

The sandbox experiments model salt migration as the prograding sediment load increases by progressive accumulation. Localized sinking of the basin, related to salt withdrawal and lateral squeezing, results in depocenters' migration in the same direction as sediment transport. Salt lateral migration may also produce salt inflation (plateau or diapir) generally favoured by the occurrence of a structural or morphological discontinuity against which the flowing material is pushed. These features are consistent overall with the syn-depositional pattern and structures observed within the turbidite basin, even if some minor differences concerning boundary conditions exist between the natural example and models (i.e., Model 1 of Rojo et al., 2020). For instance, in the natural example, Pliocene sediment thickening in the western part of the turbidite basin has been favoured by the activity of basin internal faults (i.e., the MESC system) rather than by a progradational sediment system. In the studied case, accommodation space and sediment thickening appear, in fact, to be primarily controlled by the fault activity resulting in a higher and localized sediment load approaching them. This pattern corresponds with maximum throws measured along the MESC faults (Fig. 4a, see Gambino et al., 2021).

Even if the seismic lines here presented do not provide robust constraints on the occurrence of a ductile layer flooring the investigated basin, sub-circular troughs, associated dome-shaped reliefs (Fig. 4) and uprising structures (i.e., diapirs and plateau, Fig. 6d, f), support withdrawal and inflation mechanism affecting the investigated area. Syn-depositional patterns, notably the depocenters shifting in the PQ1a sub-unit, strongly support underlying lateral migration of ductile material controlling basin shaping and evolution at least during the Pliocene. Ductile deformation during the Pliocene is in agreement with the anomalous extension rate that affected the turbidite basin at the Messinian-lower Pliocene transition as reported in Fig. 5a (see Gambino et al., 2022a). Fig. 5 highlights the main results of the 2D section restoration performed by (Gambino et al., 2022a). The cumulative extensional deformation (solid lines) observed at the Messinian-lower Pliocene transition (Fig. 5a) rapidly decreases overtime while MESC faults activity (dashed lines) maintain a relatively constant offset. To explain such a deformative trend, the authors concluded that the diffuse deformation mechanism was likely related to the presence of a ductile body underlying the investigated basin, while the relatively constant MESC faults activity represents the expression of regional tectonics.

7. Conclusions

Basin analysis performed via high-resolution seismic lines crossing a narrow turbidite basin offshore eastern Sicily provides the opportunity to better understand what processes operated in the evolution and shaping of the investigated sedimentary basin. Reflector patterns within the Pliocene units are indicative of syn-depositional deformation in response to localized basin deepening and the growth of dome-like structures in the eastern part of the basin. Depocenter shifting towards the East is unexpected considering a CAW-front pushing in the opposite-way, and clearly suggests that sediment architecture in this part of the basin was controlled by a non-tectonic deformation mechanism. 3D modelling of time-reference surfaces in the area reveals sub-circular depressions and associated culminations. This pattern resembles salt-withdrawal minibasins commonly reported in evaporite-floored basin (Goteti et al., 2012; Peel, 2014; Ge et al., 2020; Rojo et al., 2020). Long-wavelength sediment fanning driven by the extensional activity of the MESC faults and the basin sinking to the east coexisted during the Pliocene, denoting therefore that the two processes worked simultaneously to shape the internal sediment architecture of the basin. Considering that salt layers have been inferred by many studies to floor the investigated turbidite basin, we propose that salt migration was triggered by fault-controlled sediment loading with this interactive process controlling basin evolution in the Western Ionian Domain. Nevertheless, the occurrence of serpentinite-derived mud observed and inferred in the surrounding area (Manuella et al., 2012; Barreca, 2014; Polonia et al., 2017), means that the possibility of shale/mud tectonics (rather than salt) as the ductile source of deformation cannot be ruled out. This paper therefore opens stimulating research perspectives that may enable future studies on sediment patterns in salt-shale floored basins like the Mediterranean area.

Aknowledgements

Bathymetric data are from a compilation provided by Gutscher et al., (2017) and from EMODnet open dataset (http://www.emodnet-bathymetry.eu/). Digital topography was achieved from the Japan Aerospace Exploration Agency (https://www.eorc.jaxa.jp/ALOS/en/aw3d30/index.htm). The authors also acknowledge the use of MOVE Software Suite granted by Petroleum Experts Limited (www.petex.com). Bernard Mercier de Lepinay (GeoAzur, Université de Nice/CNRS), is also acknowledged for the CIRCEE-HR seismic data processing. Juan I. Soto (The University of Texas at Austin) is warmly acknowledged for the critical and constructive discussions provided. The research was partly funded by the University of Catania in the framework of the project '*SeismoFront*' (resp. G. Barreca), Grant n. 22722132176.

References

Amato, A., Azzara, R., Basili, A., Chiarabba, C., Cocco, M., Di Bona, M., & Selvaggi, G. (1995). Main shock and aftershocks of the December 13, 1990 Eastern Sicily earthquake. *Annals of Geophysics*, *38*(2), 255–266.

Argnani, A., Armigliato, A., Pagnoni, G., Zaniboni, F., Tinti, S., & Bonazzi, C. (2012). Active tectonics along the submarine slope of south-eastern Sicily and the source of the 11 January 1693 earthquake and tsunami. *Natural Hazards and Earth System Science*, *12*(5), 1311–1319. https://doi.org/10.5194/nhess-12-1311-2012

Argnani, A., & Bonazzi, C. (2005). Malta Escarpment fault zone offshore eastern Sicily: Pliocene-quaternary tectonic evolution based on new multichannel seismic data. *Tectonics*, *24*(4), 1–12. https://doi.org/10.1029/2004TC001656

Barreca, G. (2014). Geological and geophysical evidences for mud diapirism in south-eastern Sicily (Italy) and geodynamic implications. *Journal of Geodynamics*, *82*, 168–177. https://doi.org/10.1016/j.jog.2014.02.003

Barreca, G., Scarfì, L., Cannavò, F., Koulakov, I., & Monaco, C. (2016). New structural and seismological evidence and interpretation of a lithospheric-scale shear zone at the southern edge of the Ionian subduction system (central-eastern Sicily, Italy). *Tectonics*, *35*(6), 1489–1505. https://doi.org/10.1002/2015TC004057

Bianca, M., Monaco, C., Tortorici, L., & Cernobori, L. (1999). Quaternary normal faulting in southeastern Sicily (Italy): A seismic source for the 1693 large earthquake. *Geophysical Journal International*, *139*(2), 370–394. https://doi.org/10.1046/j.1365-246X.1999.00942.x

Brewer, R. C., & Kenyon, P. M. (1996). Balancing salt dome uplift and withdrawal basin subsidence in cross-section. In *Journal of Structural Geology* (Vol. 18).

Butler, R. W. H., Maniscalco, R., Sturiale, G., & Grasso, M. (2014). Stratigraphic variations control deformation patterns in evaporite basins: Messinian examples, onshore and offshore Sicily (Italy). *Journal of the Geological Society*, *172*(1), 113–124. https://doi.org/10.1144/jgs2014-024

Camerlenghi, A., Del Ben, A., Hübscher, C., Forlin, E., Geletti, R., Brancatelli, G., Micallef, A., Saule, M., & Facchin, L. (2020). Seismic markers of the Messinian salinity crisis in the deep Ionian Basin. *Basin Research*, *32*(4), 716–738. https://doi.org/10.1111/bre.12392

Catalano, R., Doglioni, C., & Merlini, S. (2001). On the Mesozoic Ionian Basin. *Geophysical Journal International*, *144*(1), 49–64. https://doi.org/10.1046/j.0956-540X.2000.01287.x

Cernobori, L., Hirn, A., McBride, J. H., Nicolich, R., Petronio, L., & Romanelli, M. (1996). Crustal image of the Ionian basin and its Calabrian margins. *Tectonophysics*, *264*(1–4), 175–189. https://doi.org/10.1016/S0040-1951(96)00125-4

Cultrera, F., Barreca, G., Scarfì, L., and Monaco, C. (2015). Fault reactivation by stress pattern reorganization in the Hyblean foreland domain of SE Sicily (Italy) and seismotectonic implications. Tectonophysics 661, 215–228. doi:10.1016/j.tecto.2015.08.043D'Agostino, N., & Selvaggi, G. (2004). Crustal motion along the Eurasia-Nubia plate boundary in the Calabrian Arc and Sicily and active extension in the Messina Straits from GPS measurements. *Journal of Geophysical Research: Solid Earth*, *109*(11), 1–16. https://doi.org/10.1029/2004JB002998

D'Agostino, N., and Selvaggi, G. (2004). Crustal motion along the eurasia-nubia plate boundary in the calabrian arc and sicily and active extension in the messina straits from GPS measurements. J. Geophys. Res. 109, B11402. doi:10.1029/2004JB002998

Dannowski, A., Kopp, H., Klingelhoefer, F., Klaeschen, D., Gutscher, M.-A., Krabbenhoeft, A., Dellong, D., Rovere, M., Graindorge, D., Papenberg, C., Papenberg, C., & Klaucke, I. (2019). Ionian Abyssal Plain: A window into the Tethys oceanic lithosphere. *Solid Earth*, *10*(2), 447–462. https://doi.org/10.5194/se-10-447-2019

De Guidi, G., Caputo, R., & Scudero, S. (2015). Regional and local stress field orientation inferred from quantitative analyses of extension joints: Case study from southern Italy. *Tectonics*, *32*(2), 239–251. https://doi.org/10.1002/tect.20017

Dellong, D., Klingelhoefer, F., Dannowski, A., Kopp, H., Murphy, S., Graindorge, D., Margheriti, L., Moretti, M., Barreca, G., Scarfì, L., Polonia, A., & Gutscher, M.-A. (2020). Reply to comment by a. Argnani on "geometry of the deep Calabrian subduction from wide-angle seismic data and 3-d gravity modeling". *Geochemistry, Geophysics, Geosystems*, *21*(8), 1–5. https://doi.org/10.1029/2020GC009223

Dellong, D., Klingelhoefer, F., Kopp, H., Graindorge, D., Margheriti, L., Moretti, M., Murphy, S., & Gutscher, M.-A. (2018). Crustal Structure of the Ionian Basin and Eastern Sicily Margin: Results From a Wide-Angle Seismic Survey. *Journal of Geophysical Research: Solid Earth*, *123*(3), 2090–2114. https://doi.org/10.1002/2017JB015312

Faccenna, C., Becker, T. W., Auer, L., Billi, A., Boschi, L., Brun, J. P., Capitanio, F. A., Funiciello, F., Horvàth, F., Jolivet, L., Rossetti, F., & Serpelloni, E. (2014). Mantle dynamics in the Mediterranean. *Reviews of Geophysics*, *52*(3), 283–332. https://doi.org/10.1002/2013RG000444

Finetti, I. (1982). Structure, stratigraphy and evolution of central Mediterranean (Pelagian Sea, Ionian Sea). *Bollettino di Geofisica Teorica ed Applicata*, *24*(96), 247–312.

Gallais, F., Gutscher, M.-A., Graindorge, D., Chamot-Rooke, N., & Klaeschen, D. (2011). A Miocene tectonic inversion in the Ionian Sea (central Mediterranean): Evidence from multichannel seismic data. *Journal of Geophysical Research: Solid Earth*, *116*(12). https://doi.org/10.1029/2011JB008505

Gallais, F., Gutscher, M. A., Klaeschen, D., & Graindorge, D. (2012). Two-stage growth of the Calabrian accretionary wedge in the Ionian Sea (Central Mediterranean): Constraints from depth-migrated multichannel seismic data. *Marine Geology*, *326–328*, 28–45. https://doi.org/10.1016/J.MARGEO.2012.08.006

Gambino, S., Barreca, G., Bruno, V., De Guidi, G., Ferlito, C., Gross, F., Mattia, M., Scarfì, L., & Monaco, C. (2022b). Transtension at the Northern Termination of the Alfeo-Etna Fault System (Western Ionian Sea, Italy): Seismotectonic Implications and Relation with Mt. Etna Volcanism. *Geosciences*, *12*(3), 128. https://doi.org/10.3390/geosciences12030128

Gambino, S., Barreca, G., Gross, F., Monaco, C., Gutscher, M. A., & Alsop, G. I. (2022a). Assessing the rate of crustal extension by 2D sequential restoration analysis: A case study from the active portion of the Malta Escarpment. *Basin Research*, *34*(1), 321–341. https://doi.org/10.1111/bre.12621

Gambino, S., Barreca, G., Gross, F., Monaco, C., Krastel, S., & Gutscher, M. A. (2021). Deformation pattern of the northern sector of the malta escarpment (Offshore SE Sicily, Italy): Fault dimension, slip prediction, and seismotectonic implications. *Frontiers in Earth Science*, *8*, 1–20. https://doi.org/10.3389/feart.2020.594176

Ge, Z., Gawthorpe, R. L., Rotevatn, A., Zijerveld, L., A.-L. Jackson, C., & Oluboyo, A. (2020). Minibasin depocentre migration during diachronous salt welding, offshore Angola. *Basin Research*, *32*(5), 875–903. https://doi.org/10.1111/bre.12404

Gemmer, L., Ings, S. J., Medvedev, S., & Beaumont, C. (2004). Salt tectonics driven by differential sediment loading: Stability analysis and finite-element experiments. *Basin Research*, *16*(2), 199–218. https://doi.org/10.1111/j.1365-2117.2004.00229.x

Goteti, R., Ings, S. J., & Beaumont, C. (2012). Development of salt minibasins initiated by sedimentary topographic relief. *Earth and Planetary Science Letters*, *339–340*, 103–116. https://doi.org/10.1016/j.epsl.2012.04.045

Govers, R., & Wortel, M. J. R. (2005). Lithosphere tearing at STEP faults: Response to edges of subduction zones. *Earth and Planetary Science Letters*, *236*(1–2), 505–523. https://doi.org/10.1016/j.epsl.2005.03.022

Grenerczy, G., Sella, G., Stein, S., and Kenyeres, A. (2005). Tectonic implications of the GPS velocity field in the northern Adriatic region. Geophys. Res. Lett. 32, L16311. doi:10.1029/2005GL022947

Gutscher, M.-A., Dominguez, S., De Lepinay, B. M., Pinheiro, L., Gallais, F., Babonneau, N., Cattaneo, A., Le Faou, Y., Barreca, G., Micallef, A., Micallef, A., & Rovere, M. (2016). Tectonic expression of an active slab tear from high-resolution seismic and bathymetric data offshore Sicily (Ionian Sea). *Tectonics*, *35*(1), 39–54. https://doi.org/10.1002/2015TC003898

Gutscher, M.-A., Kopp, H., Krastel, S., Bohrmann, G., Garlan, T., Zaragosi, S., Klaucke, I., Wintersteller, P., Loubrieu, B., Le Faou, Y., Ranero, C., & Sallares, V. (2017). Active tectonics of the Calabrian subduction revealed by new multi-beam bathymetric data and high-resolution seismic profiles in the Ionian Sea (Central Mediterranean). *Earth and Planetary Science Letters*, *461*, 61–72. https://doi.org/10.1016/j.epsl.2016.12.020

Hsü, K. J., Montadert, L., Bernoulli, D., Bizon, G., Cita, M., Erickson, A., & et al. (1978). *Site 374: Messina Abyssal plain Part 1." in Initial Reports of the Deep-Sea Drilling Project*.

Hsü, K. J., Montadert, L., Bernoulli, D., Cita, M. B., Erickson, A., Garrison, R. E., Kidd, R. B., Mèlierés, F., Müller, C., & Wright, R. (1977). History of the mediterranean salinity crisis. *Nature*, *267*(5610), 399–403. https://doi.org/10.1038/267399a0

Hudec, M. R., Jackson, M. P. A., & Schultz-Ela, D. D. (2009). The paradox of minibasin subsidence into salt: Clues to the evolution of crustal basins. *Bulletin of the Geological Society of America*, *121*(1–2), 201–221. https://doi.org/10.1130/B26275.1

Jolivet, L., & Faccenna, C. (2000). Medditerranean extension and the Africa-Eurasia collision. *Tectonics*, *19*(6), 1095–1106. https://doi.org/10.1029/2000TC900018

Kokinou, E., Vafidis, A., Loucogiannakis, M., & Louis, I. (2003). Deep Seismic Imaging and Velocity Estimation in Ionian Sea. *Journal of the Balkan Geophysical Society*. *6*(2), 100–116. http://www.balkangeophysoc.gr/online-journal/2003_V6/may2003/Louis_1_Mike.PDF

Krastel, S. (2016). *RV POSEIDON-CRUISE POS496, Malaga – Catania, 24.03.2016 - 04.04.2016, Short Cruise Report: MAGOMET - Offshore flank movement of Mount Etna and associated landslide hazard in the Ionian Sea (Mediterranean Sea)*.

Lofi, J., Sage, F., Déverchère, J., Loncke, L., Maillard, A., Gaullier, V., Thinon, I., Gillet, H., Guennoc, P., & Gorini, C. (2011). Refining our knowledge of the Messinian salinity crisis records in the offshore domain through multi-site seismic analysis. *Bulletin de la Société Géologique de France*, *182*(2), 163–180. https://doi.org/10.2113/gssgfbull.182.2.163

Loncke, L., Gaullier, V., Mascle, J., Vendeville, B., & Camera, L. (2006). The Nile deep-sea fan: An example of interacting sedimentation, salt tectonics, and inherited subsalt paleotopographic features. *Marine and Petroleum Geology*, *23*(3), 297–315. https://doi.org/10.1016/j.marpetgeo.2006.01.001

Lopez-Mir, B., Anton Muñoz, J., & García Senz, J. (2014). Restoration of basins driven by extension and salt tectonics: Example from the Cotiella Basin in the central Pyrenees. *Journal of Structural Geology*, *69*(PA), 147–162. https://doi.org/10.1016/j.jsg.2014.09.022

Maesano, F. E., Tiberti, M. M., & Basili, R. (2017). The Calabrian Arc: Three-dimensional modelling of the subduction interface. *Scientific Reports*, *7*(1). https://doi.org/10.1038/s41598-017-09074-8

Maesano, F. E., Tiberti, M. M., and Basili, R. (2020). Deformation and fault propagation at the lateral termination of a subduction zone: the alfeo Fault system in the calabrian arc, southern Italy. Front. Earth Sci. 8, 107. doi:10.3389/feart.2020.00107

Malinverno, A., & Ryan, W. B. F. (1986). Extension in the Tyrrhenian Sea and shortening in the Apennines as result of arc migration driven by sinking of the lithosphere. *Tectonics*, *5*(2), 227–245. https://doi.org/10.1029/TC005i002p00227

Manuella, F. C., Carbone, S., & Barreca, G. (2012). Origin of saponite-rich clays in a fossil serpentinite-hosted hydrothermal system in the crustal basement of the Hyblean Plateau (Sicily, Italy). *Clays and Clay Minerals*, *60*(1), 18–31. https://doi.org/10.1346/CCMN.2012.0600102

Mastrolembo, V. B., Serpelloni, E., Argnani, A., Bonforte, A., Bürgmann, R., Anzidei, M. P., et al. (2014). Fast geodetic strain-rates in eastern sicily (southern Italy): new insights into block tectonics and seismic potential in the area of the great 1693 earthquake. Earth Planet Sci. Lett. 404, 77–88. doi:10.1016/j.epsl.2014.07.025

Mattia, M., Bruno, V., Cannavò, F., & Palano, M. (2012). Evidences of a contractional pattern along the northern rim of the Hyblean plateau (Sicily, Italy) from GPS data. *Geologica Acta*, *10*(1), 63–70. https://doi.org/10.1344/105.000001705

Meschis, M., Scicchitano, G., Roberts, G. P., Robertson, J., Barreca, G., Monaco, C., ... & Scardino, G. (2020). Regional deformation and offshore crustal local faulting as combined processes to explain uplift through time constrained by investigating differentially uplifted late quaternary paleoshorelines: The foreland Hyblean plateau, SE Sicily. Tectonics, 39(12), e2020TC006187. https://doi.org/10.1029/2020TC006187

Micallef, A., Camerlenghi, A., Garcia-Castellanos, D., Cunarro Otero, D., Gutscher, M.-A., Barreca, G., Spatola, D., Facchin, L., Geletti, R., Krastel, S., Gross, F., & Urlaub, M. (2018). Evidence of the Zanclean megaflood in the eastern Mediterranean Basin. *Scientific Reports*, *8*(1). https://doi.org/10.1038/s41598-018-19446-3

Minelli, L., & Faccenna, C. (2010). Evolution of the Calabrian accretionary wedge (central Mediterranean). *Tectonics*, *29*(4), 1–21. https://doi.org/10.1029/2009TC002562

Monaco, C., & Tortorici, L. (2000). Active faulting in the Calabrian arc and eastern Sicily. *Journal of Geodynamics*, *29*(3–5), 407–424. https://doi.org/10.1016/S0264-3707(99)00052-6

Montone, P., Mariucci, M. T., & Pierdominici, S. (2012). The Italian present-day stress map. *Geophysical Journal International*, *189*(2), 705–716. https://doi.org/10.1111/j.1365-246X.2012.05391.x

Morley, C. K., & Guerin, G. (1996). Comparison of gravity-driven deformation styles and behavior associated with mobile shales and salt. In *Tectonics* (Vol. 15, Numero 6, pagg. 1154–1170). American Geophysical Union. https://doi.org/10.1029/96TC01416

Palano, M., Ferranti, L., Monaco, C., Mattia, M., Aloisi, M., Bruno, V., Cannav, F., & Siligato, G. (2012). GPS velocity and strain fields in Sicily and southern Calabria, Italy: Updated geodetic constraints on tectonic block interaction in the central Mediterranean. *Journal of Geophysical Research: Solid Earth*, *117*(7). https://doi.org/10.1029/2012JB009254

Peel, F. J. (2014). How do salt withdrawal minibasins form? Insights from forward modelling, and implications for hydrocarbon migration. *Tectonophysics*, *630*(C), 222–235. https://doi.org/10.1016/j.tecto.2014.05.027

Polonia, A., Torelli, L., Artoni, A., Carlini, M., Faccenna, C., Ferranti, L., Gasperini, L., Govers, R., Klaeschen, D., Monaco, C., Orecchio, B., & Wortel, R. (2016). The Ionian and Alfeo-Etna fault zones: New segments of an evolving plate boundary in the central Mediterranean Sea? *Tectonophysics*, *675*, 69–90. https://doi.org/10.1016/j.tecto.2016.03.016

Polonia, A., Torelli, L., Gasperini, L., Cocchi, L., Muccini, F., Bonatti, E., Hensen, C., Schmidt, M., Romano, S., Artoni, A., Artoni, A., & Carlini, M. (2017). Lower plate serpentinite diapirism in the Calabrian Arc subduction complex. *Nature Communications*, *8*(1). https://doi.org/10.1038/s41467-017-02273-x

Polonia, A., Torelli, L., Mussoni, P., Gasperini, L., Artoni, A., & Klaeschen, D. (2011). The Calabrian Arc subduction complex in the Ionian Sea: Regional architecture, active deformation, and seismic hazard. *Tectonics*, *30*(5). https://doi.org/10.1029/2010TC002821

Ragg, S., Grasso, M., & Müller, B. (1999). Patterns of tectonic stress in Sicily from borehole breakout observations and finite element modeling. *Tectonics*, *18*(4), 669–685. https://doi.org/10.1029/1999TC900010

Rebesco, M., Camerlenghi, A., Munari, V., Mosetti, R., Ford, J., Micallef, A., & Facchin, L. (2021). Bottom current-controlled Quaternary sedimentation at the foot of the Malta Escarpment (Ionian Basin, Mediterranean). *Marine Geology*, *441*, 106596. https://doi.org/10.1016/j.margeo.2021.106596

Reiche, S., Hübscher, C., & Beitz, M. (2014). Fault-controlled evaporite deformation in the Levant Basin, Eastern Mediterranean. *Marine Geology*, *354*, 53–68. https://doi.org/10.1016/j.margeo.2014.05.002

Rojo, L. A., Koyi, H., Cardozo, N., & Escalona, A. (2020). Salt tectonics in salt-bearing rift basins: Progradational loading vs extension. *Journal of Structural Geology*, *141*. https://doi.org/10.1016/j.jsg.2020.104193

Rosenbaum, G., Gasparon, M., Lucente, F. P., Peccerillo, A., & Miller, M. S. (2008). Kinematics of slab tear faults during subduction segmentation and implications for Italian magmatism. *Tectonics*, *27*(2). https://doi.org/10.1029/2007TC002143

Rowan, M. G., & Ratliff, R. A. (2012). Cross-section restoration of salt-related deformation: Best practices and potential pitfalls. In *Journal of Structural Geology* (Vol. 41, pagg. 24–37). https://doi.org/10.1016/j.jsg.2011.12.012

Scandone, P. (1981). Mesozoic and Cenozoic rocks from the Malta Escarpment (central Mediterranean). *American Association of Petroleum Geologists Bulletin*, *65*(7), 1299–1319. https://doi.org/https://doi.org/10.1306/03B5949F-16D1-11D7-8645000102C1865D

Scarfì, L., Barberi, G., Barreca, G., Cannavò, F., Koulakov, I., & Patanè, D. (2018). Slab narrowing in the Central Mediterranean: The Calabro-Ionian subduction zone as imaged by high resolution seismic tomography. *Scientific Reports*, *8*(1). https://doi.org/10.1038/s41598-018-23543-8

Schellart, W. P., Freeman, J., Stegman, D. R., Moresi, L., & May, D. (2007). Evolution and diversity of subduction zones controlled by slab width. *Nature*, *446*(7133), 308–311. https://doi.org/10.1038/nature05615

Scicchitano, G., Gambino, S., Scardino, G., Barreca, G., Gross, F., Mastronuzzi, G., & Monaco, C. (2022). The enigmatic 1693 AD tsunami in the eastern Mediterranean Sea: new insights on the triggering mechanisms and propagation dynamics. Scientific Reports, 12(1), 9573. https://doi.org/10.1038/s41598-022-13538-x

Şengör, A. M. C. (1979). Mid-Mesozoic closure of Permo-Triassic Tethys and its implications. *Nature*, *279*(5714), 590–593. https://doi.org/10.1038/279590a0

Soto, J. I., Déverchère, J., Hudec, M. R., Medaouri, M., Badji, R., Gaullier, V., & Leffondré, P. (2022). Crustal structures and salt tectonics on the margins of the western Algerian Basin (Mediterranean Region). *Marine and Petroleum Geology*, *144*. https://doi.org/10.1016/j.marpetgeo.2022.105820

Soto, J. I., Fernández-lbáñez, F., Talukder, A. R., & Martínez-García, P. (2010). Miocene shale tectonics in the northern Alboran Sea (Western Mediterranean). *AAPG Memoir*, *93*, 119–144. https://doi.org/10.1306/13231312M933422

Soto, J. I., Heidari, M., & Hudec, M. R. (2021). Proposal for a mechanical model of mobile shales. *Scientific Reports*, *11*(1). https://doi.org/10.1038/s41598-021-02868-x

Speranza, F., Minelli, L., Pignatelli, A., & Chiappini, M. (2012). The Ionian Sea: The oldest in situ ocean fragment of the world? *Journal of Geophysical Research: Solid Earth*, *117*(12). https://doi.org/10.1029/2012JB009475

Tugend, J., Chamot-Rooke, N., Arsenikos, S., Blanpied, C., & Frizon de Lamotte, D. (2019). Geology of the Ionian Basin and Margins: A Key to the East Mediterranean Geodynamics. *Tectonics*, *38*(8), 2668–2702. https://doi.org/10.1029/2018TC005472

Valenti, V. (2010). Shallow structures at the outer Calabrian accretionary wedge (NW Ionian Sea): New insights from recently migrated reflection data. *Terra Nova*, *22*(6), 453–462. https://doi.org/10.1111/j.1365-3121.2010.00964.x

Ward, S. (1994). Constraints on the seismotectonics of the central mediterranean from very long baseline interferometry. Geophys. J. Int. 117, 441–452. doi:10.1111/j.1365-246X.1994.tb03943.x

Wiener, R. W., Mann, M. G., Angelich, M. T., & Molyneux, J. B. (2010). Mobile shale in the Niger Delta: Characteristics, structure, and evolution. *AAPG Memoir*, *93*, 145–161. https://doi.org/10.1306/13231313M933423

Wood, L. J. (2010). Shale tectonics: A preface. *AAPG Memoir*, *93*, 1–4. https://doi.org/10.1306/13231305M93730

Figure captions

Fig. 1 - (a) Structural setting of the Calabrian Accretionary Wedge and Eastern Sicily. (b) The investigated turbidite basin in the framework of the Western Ionian Basin. MESC: Malta Escarpment, NAF: North Alfeo Fault (c) Location of seismic profiles offshore Eastern Sicily used for the 3D modeling of reference surfaces (see also Argnani and Bonazzi, 2005; Argnani et al., 2012; Gutscher et al., 2016; Polonia et al., 2016, 2017). White arrows indicate the main direction of sediment supply in the investigated area. (d-e) Schematic (not to scale) crustal profiles across the Western Ionian basin. Fig. 1a-c modified from Gambino et al., (2021b).

Fig. 2 - (a) Seismo-stratigraphic interpretation of the Cir-01 seismic line (see location in Fig. 1c) following Gambino et al., (2021). (b) Details of the subsided area (trough) in the easternmost sector of the investigated turbidite basin. (c) Line-drawing of the subsided area showing the internal seismo-stratigraphic pattern and reflectors' lateral termination within PQ1 and PQ2 units.

Fig. 3 - The p701 profile (see location in Fig. 1c) crossing longitudinally the turbidite basin and showing the Plio-Quaternary stratigraphic pattern dominated by sediment waves. The latter, indicate sediment discharging toward the SE.

Fig. 4 - a) Cumulative throw-distance diagram of the MESC faults (F1, F2, F3, see Gambino et al., 2021).(b) Contour-coloured map of the interpolated S2 (top-MES) 3D surface. Troughs are located where faults maximum throws are measured, whereas domes are located along the NAF system. (c) Contour-coloured map of the interpolated S3 (top-PQ1) 3D surface. (d) Thickness map of the PQ1 units between S2 and S3 surfaces.

Fig. 5 - (a) Displacement curves (horizontal and vertical components) of faults within the Cir-01 line according to (Gambino et al., 2022a). A relatively constant activity is observed for MESC faults (dashed lines), while a diffuse extension (red solid line) is observed to decrease from lower Pliocene to Quaternary. (b) Schematic model of the Cir-01 seismic line exploited for back-restoration (see Gambino et al., 2022a). (c) Restored Cir-01 seismic line at Upper Messinian time.

Fig. 6 - (a) Location of seismic lines p202 and Cir-01 in the framework of the Western Ionian Basin (b) Portion of Cir-01 showing the internal subdivision of MES unit (see also Gutscher et al., 2016 and Gambino et al., 2021) (c-d) Comparison and similarity between the sand-box model predicting ductile migration under sediment loading (inverted view) proposed by Rojo et al., (2020), and the line-drawing of Cir-01 profile. (e-f) Comparison between the same sand-box model and the line-drawing of the p202 profile showing the occurrence of uprising material along a distal fault (for the original seismic image of the p202 see Gambino et al., 2022b). This distal fault in the case proposed is only supposed since the analyzed seismic lines does not extend far enough

Tab.1 – Seismic velocities and physical parameters (from Gambino et al., 2022a) of seismic units used for TWT-Depth conversion.

Tab.1

	Seismic Unit	Age	Age (Ma)	Lithology	Seismic Velocity (m/s)	Surface porosity	Density (km/m^3)	Depth Coeff. (km^{-1})	References
	PQ2	Quaternary	2.58-0.012	Silty-sandstones	1760	0.4	2700	0.39	Micallef et al., 2018
PQ1	c	Upper Pliocene	3.6-2.58	Silty-sandstones	2280	0.4	2700	0.39	Micallef et al., 2018; Camerlenghi et al., 2020
	b	Upper/Lower Pliocene	4.0-3.6	Silty-sandstones	2280	0.4	2700	0.39	
	a	Lower Pliocene	5.3-4.0	Silty-sandstones	2280	0.4	2700	0.39	
	MES	Messinian	7.2-5.3	Evaporites	4000	0	2200	0.00	Butler et al., 2014; Maesano et al., 2017
	Pre-MES	Pre-Messinian	up to 7.2	Limestones	3250	0.7	2700	0.71	Gallais et al., 2011; Kokinou et al., 2003; Micallef et al., 2018

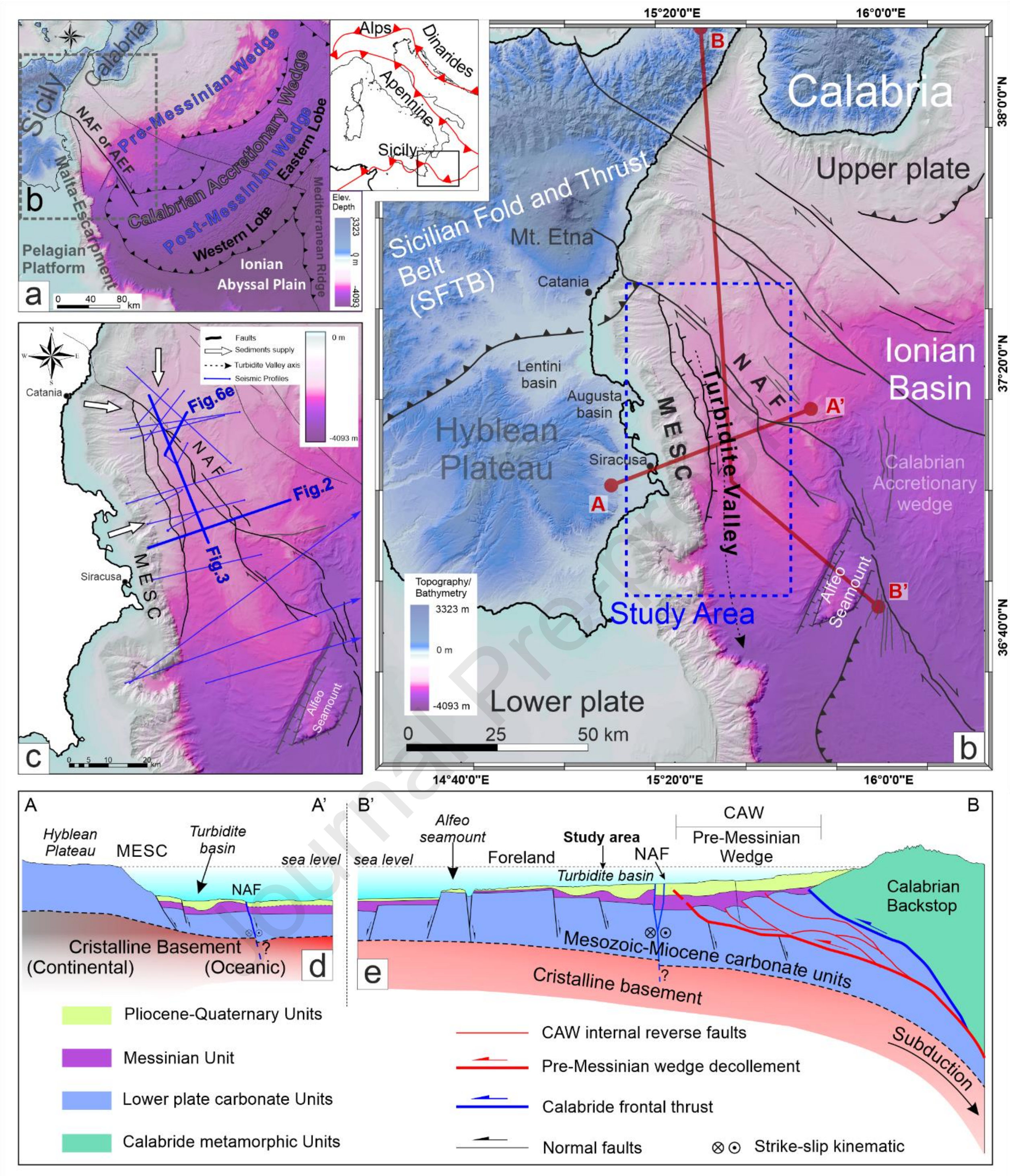

Fig. 1. (a) Structural setting of the Calabrian Accretionary Wedge and Eastern Sicily. (b) The investigated turbidite basin in the framework of the Western Ionian Basin. MESC: Malta Escarpment, NAF: North Alfeo Fault (c) Location of seismic profiles offshore Eastern Sicily used for the 3D modeling of reference surfaces (see also Argnani and Bonazzi, 2005; Argnani et al., 2012; Gutscher et al., 2016; Polonia et al., 2016, 2017). White arrows indicate the main direction of sediment supply in the investigated area. (d-e) Schematic (not to scale) crustal profiles across the Western Ionian basin. Fig. 1a-c modified from Gambino et al., (2021b).

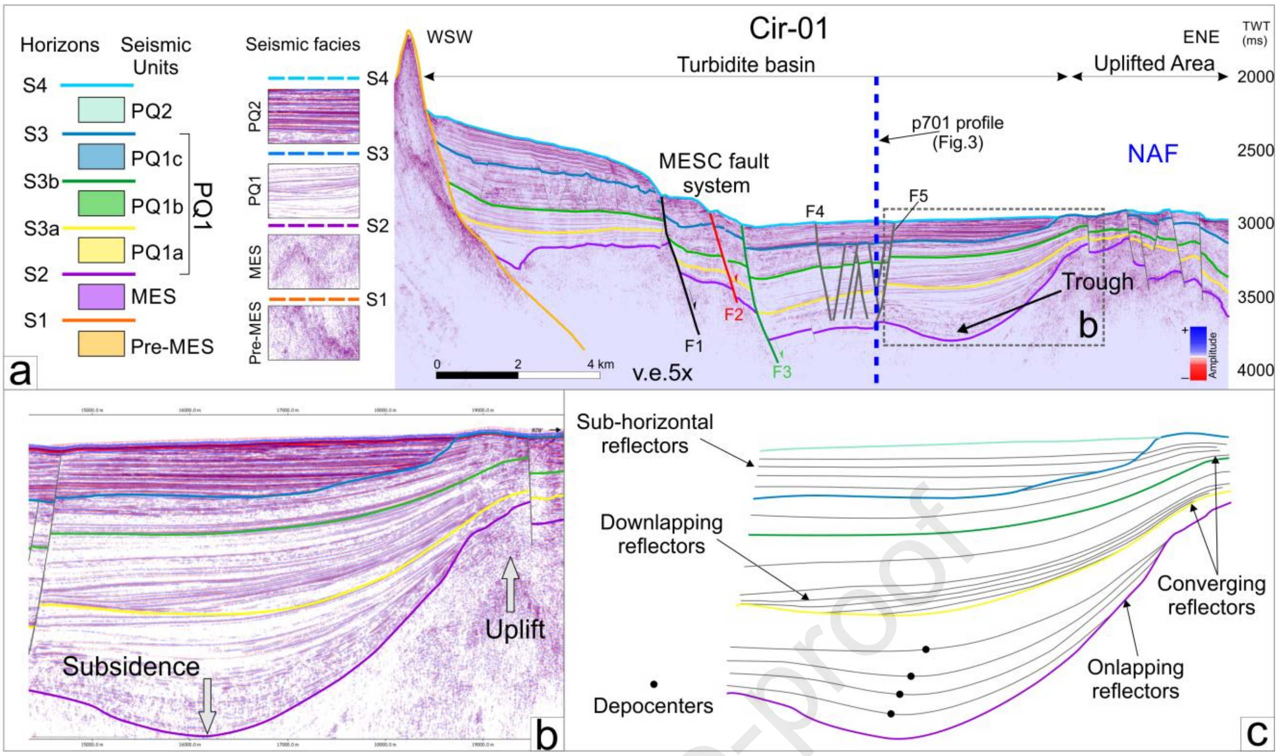

Fig. 2. (a) Seismo-stratigraphic interpretation of the Cir-01 seismic line (see location in Fig. 1c) following Gambino et al., (2021). (b) Details of the subsided area (trough) in the easternmost sector of the investigated turbidite basin. (c) Line-drawing of the subsided area showing the internal seismo-stratigraphic pattern and reflectors' lateral termination within PQ1 and PQ2 units.

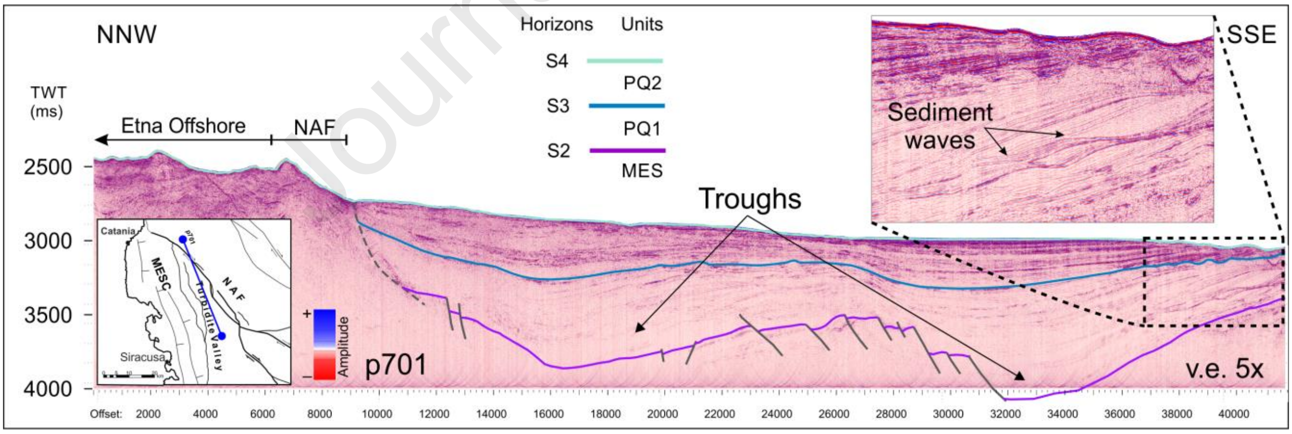

Fig. 3. The p701 profile (see location in Fig. 1c) crossing longitudinally the turbidite basin and showing the Plio-Quaternary stratigraphic pattern dominated by sediment waves. The latter, indicate sediment discharging toward the SE.

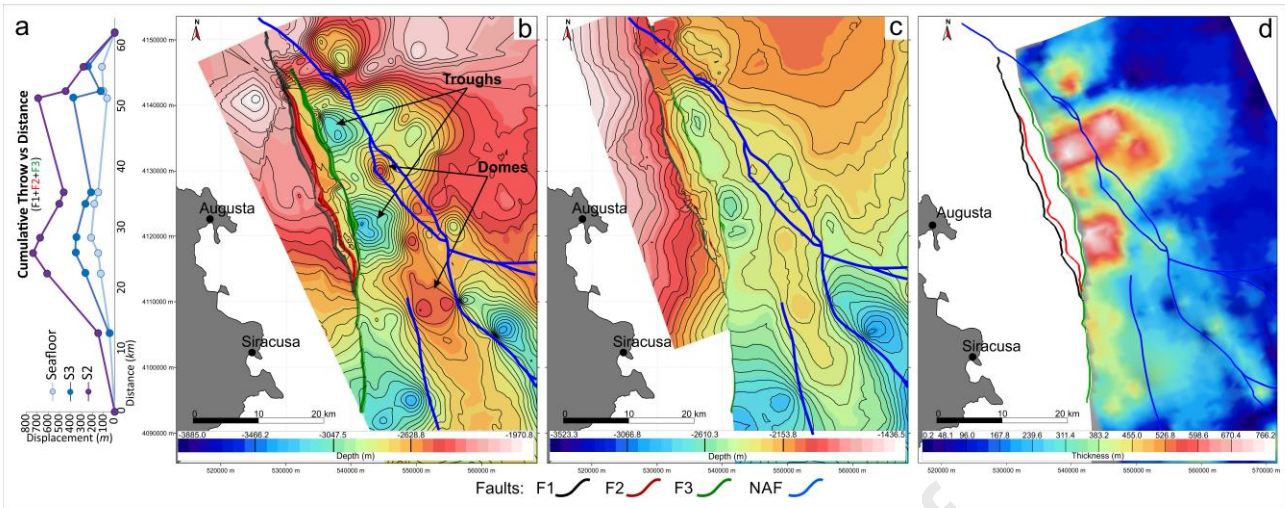

Fig. 4. a) Cumulative throw-distance diagram of the MESC faults (F1, F2, F3, see Gambino et al., 2021).(b) Contour-coloured map of the interpolated S2 (top-MES) 3D surface. Troughs are located where faults maximum throws are measured, whereas domes are located along the NAF system. (c) Contour-coloured map of the interpolated S3 (top-PQ1) 3D surface. (d) Thickness map of the PQ1 units between S2 and S3 surfaces.

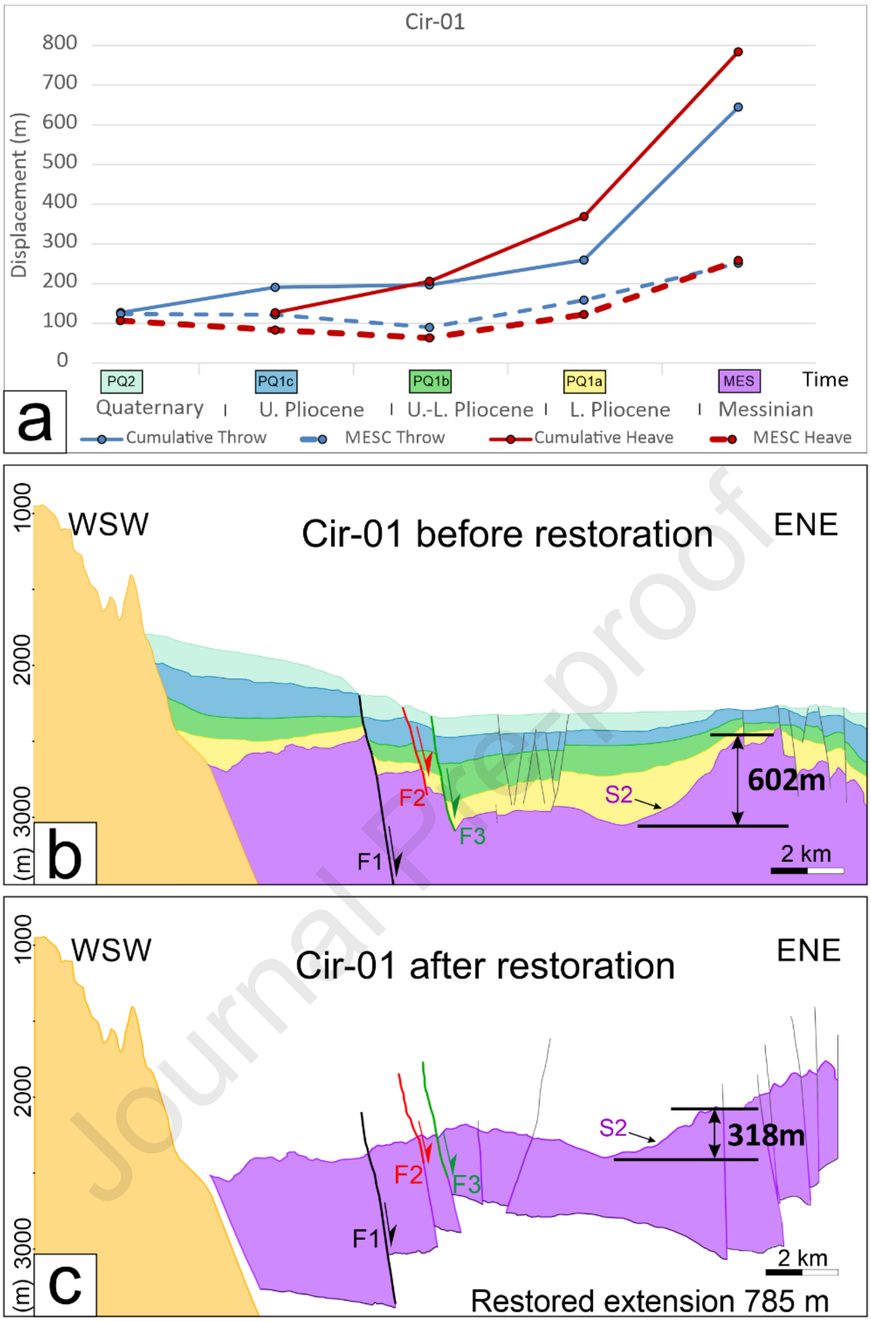

Fig. 5. (a) Displacement curves (horizontal and vertical components) of faults within the Cir-01 line according to (Gambino et al., 2022a). A relatively constant activity is observed for MESC faults (dashed lines), while a diffuse extension (red solid line) is observed to decrease from lower Pliocene to Quaternary. (b) Schematic model of the Cir-01 seismic line exploited for back-restoration (see Gambino et al., 2022a). (c) Restored Cir-01 seismic line at Upper Messinian time.

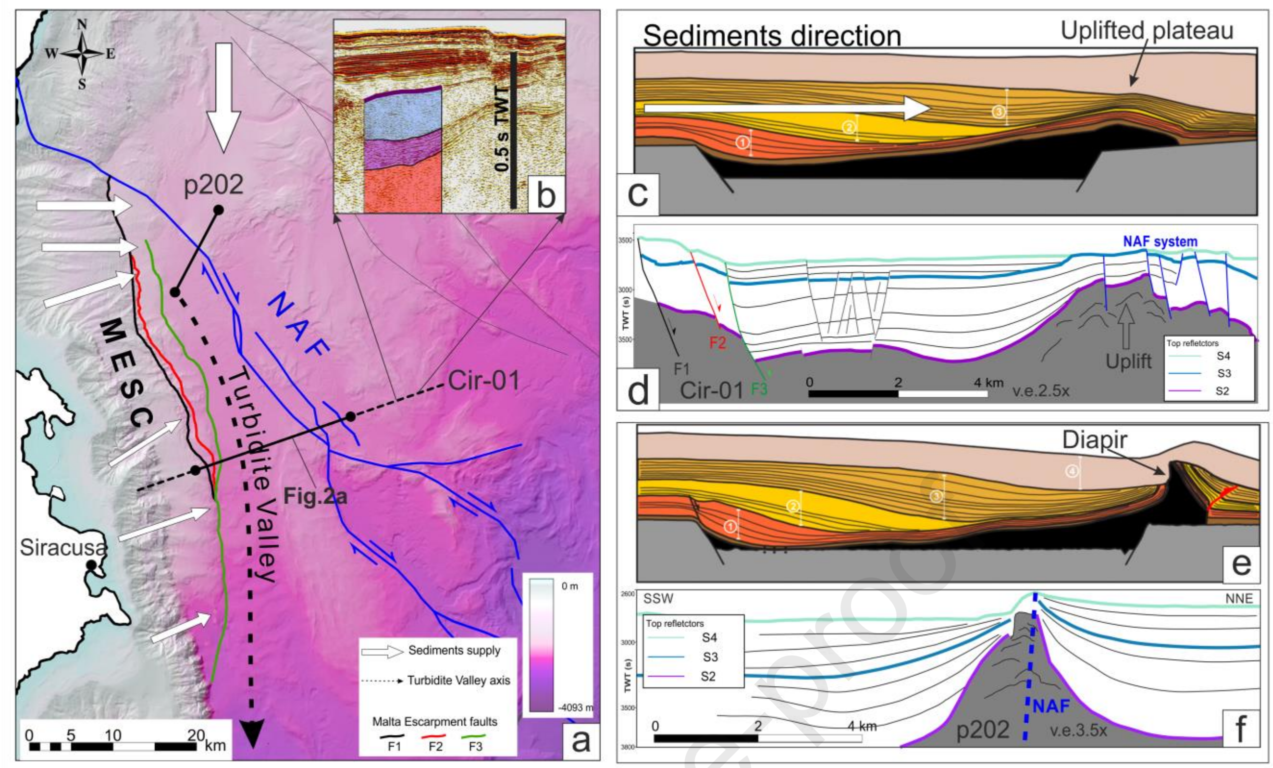

Fig. 6. (a) Location of seismic lines p202 and Cir-01 in the framework of the Western Ionian Basin (b) Portion of Cir-01 showing the internal subdivision of MES unit (see also Gutscher et al., 2016 and Gambino et al., 2021) (c-d) Comparison and similarity between the sand-box model predicting ductile migration under sediment loading (inverted view) proposed by Rojo et al., (2020), and the line-drawing of Cir-01 profile. (e-f) Comparison between the same sand-box model and the line-drawing of the p202 profile showing the occurrence of uprising material along a distal fault (for the original seismic image of the p202 see Gambino et al., 2022b). This distal fault in the case proposed is only supposed since the analyzed seismic lines does not extend far enough

	Seismic Unit	Age	Age (Ma)	Lithology	Seismic Velocity (m/s)	Surface porosity	Density (km/m^3)	Depth Coeff. (km^{-1})	References
	PQ2	Quaternary	2.58-0.012	Silty-sandstones	1760	0.4	2700	0.39	Micallef et al., 2018
PQ1	c	Upper Pliocene	3.6-2.58	Silty-sandstones	2280	0.4	2700	0.39	Micallef et al., 2018; Camerlenghi et al., 2020
	b	Upper/Lower Pliocene	4.0-3.6	Silty-sandstones	2280	0.4	2700	0.39	
	a	Lower Pliocene	5.3-4.0	Silty-sandstones	2280	0.4	2700	0.39	
	MES	Messinian	7.2-5.3	Evaporites	4000	0	2200	0.00	Butler et al., 2014; Maesano et al., 2017
	Pre-MES	Pre-Messinian	up to 7.2	Limestones	3250	0.7	2700	0.71	Gallais et al., 2011; Kokinou et al., 2003; Micallef et al., 2018

Tab.1. Seismic velocities and physical parameters (from Gambino et al., 2022a) of seismic units used for TWT-Depth conversion.

Highlights

- Faults activity provided localized sediments loading
- Sediments loading triggered flow of underlying ductile material
- Simultaneous subsidence and uplift affected the Pliocene section
- 3D model provides indication of a dome-and-basin structures
- Circular-shaped basins resemble withdrawal mini-basins

Declaration of interests

☒ The authors declare that they have no known competing financial interests or personal relationships that could have appeared to influence the work reported in this paper.

☐ The authors declare the following financial interests/personal relationships which may be considered as potential competing interests: